Chapter 5

Investigation of Epitaxial (0002) ZnCoO Films with Antiferromagnetic Layer NiO

5.1 Introduction

In this chapter, the first section would describe the fabrication of ZnCoO with metallic underlayer. Meanwhile, we would discuss the crystalline, magnetic, and surface properties of ZnCoO films grown on the Cu underlayer at room-temperature.

A diluted magnetic semiconductor (DMS) is one of the promising candidates for spintronic devices due to its capability of manipulating both degrees of freedoms of electrons' spins and charges [1-2]. Theoretical investigations predicted that TM-doped ZnO might possess room-temperature ferromagnetism [3]. However, the origin of ferromagnetism in these materials is still somewhat controversial. Several reports supported the mechanism of intrinsically carrier-mediated ferromagnetism [3-4] while others claimed that of magnetic-cluster-induced ferromagnetism [5]. On the other hand, the theory of percolation of bound magnetic polarons has also been proposed to explain the origin of ferromagnetism in oxide-based DMSs [6-8]. The carrier-mediated ferromagnetism requires the presence of a certain level of carrier concentration, whereas the bound magnetic polaron model can be applicable to the insulating state.

The elevated deposition temperature and specific single-crystal substrates are typically required to obtain good-quality ZnCoO films, which may increase the complexity for future fabrication of multilayer spintronic devices. In this study, we grew textured and epitaxial ZnCoO films on Si wafers at room temperature by using an ion beam deposition (IBD) system. The relationships among oxygen flow rate during deposition, carrier concentrations, saturation magnetization and magneto-transport properties are discussed. We report ZnCoO films with high carrier concentrations of $10^{19}/cm^3$, which may be required for applications. Furthermore, we demonstrate room-temperature ferromagnetism of epitaxial (0002) $ZnCo_{0.07}O$ films by growing them on Cu underlayers.

On the other hand, to integrate DMSs into spintronic devices, an exchange-biasing scheme is quite important. Exchange coupling between a DMS ($Ga_{1-x}Mn_xAs$) and an antiferromagnet (MnO) has been reported [9], however, very limited work has been reported on the exchange bias of oxide-DMS systems. In the second section, we report the exchange bias between epitaxially-grown $ZnCo_{0.07}O$ and NiO.

The unidirectional anisotropy in a ferromagnetic (FM)/AFM system has been reported to be a consequence of interfacial exchange coupling between FM and pinned uncompensated AFM spins [10]. Uncompensated spins on the surface of AFM CoO films has been reported, which reasonably explained the reduction of exchange field compared to the ideal interface model [11]. In Ohldag's studies, x-ray magnetic circular dichroism (XMCD) was performed to identify the Mn spin moment within the Co/IrMn bilayer system [12]. The hysteresis

loop of Mn spins revealed a vertical magnetization shift, suggesting that part of the uncompensated AFM spins may not be reversed by the relatively small measuring field. However, it is difficult to directly observe the vertical magnetization shift with conventionally measured FM/AFM hysteresis loops. This is because the typical magnetization of FM films is too large to reveal the existence of the pinned interfacial spins. On the other hand, vertical magnetization shifts have been reported in several nanoparticle core-shell systems due to the high interfacial area to volume ratio [13]. DMSs have much lower magnetization than typical FM films, which may enable us to investigate the role of the pinned spins in exchange-bias systems by measuring conventional hysteresis loops. In the second section, we report both vertical and horizontal shifts in the hysteresis loops of ZnCoO/NiO bilayers measured with a superconducting quantum interference device (SQUID). We discuss the relationship between exchange-bias fields and the vertical magnetization shifts in the ZnCoO/NiO bilayers to elucidate the role of the pinned spins in the exchange-bias system

5.2 Experimental Procedures

ZnCoO (40 nm) films were grown on Si (001) substrates with 200 nm SiO_2 or 40 nm Cu layers at room temperature by using an ion beam deposition system. The base pressure of IBD was 2×10^{-7} Torr and the working pressure was maintained at 3×10^{-4} Torr. A composite target composed of a Zn target and Co chips was used for ZnCoO deposition. During the ZnCoO deposition, Ar (6 sccm) and O_2 (2 or 3.2 sccm) were simultaneously introduced. To study exchange bias, samples of Cu 40 nm/ZnCoO 40 nm/ NiO 50 nm were fabricated at room temperature. Film structures were characterized by an X-ray diffractometer (XRD). The valence state of Co was identified with X-ray photoelectron spectroscopy (XPS) at scanning photoelectron microscope (SPEM) station in the National Synchrotron Radiation Research Center (NSRRC), Co concentration of ZnCoO films was determined by inductively coupled plasma-mass spectrometry (ICP-MS). Hysteresis loops were measured with a SQUID with either a zero-field-cooling (ZFC) or field-cooling (FC) process. The FC process was performed by applying a field in the direction of the film plane at room temperature, and then cooling the samples down to 5 K. Magneto-transport properties were investigated by using a physical property measurement system (PPMS). Carrier concentrations were obtained by using the van der Pauw method of Hall measurement with a constant out-of-plane magnetic field of 5500 Oe at room temperature. Dark-field images of transmission electron microscopy (TEM) and diffraction patterns were taken to verify the characteristics of epitaxial ZnCoO films.

5.3 Results and Discussions

5.3.a Fabrication of Epitaxial (0002) ZnCoO Films with Cu underlayer

The Co concentration of ZnCoO is 7 % ($ZnCo_{0.07}O$). The XRD patterns, as shown in Fig.5.1 (a) and Fig.5.1 (b), indicated a good out-of-plane (0002) texture of ZnCoO films on SiO_2 and on (002) Cu underlayers, respectively. No second phases were observed in XRD patterns.

For future applications of spintronic devices, high-quality epitaxial DMS films grown on Si wafers with high carrier concentrations may be preferred. To obtain the epitaxial ZnCoO films, we used a Cu layer as the underlayer for ZnCoO growth. The Cu (001) epitaxial films were reported to grow epitaxially on hydrogen terminated (1×1) Si (001) reconstructed surface [14], and was used as underlayers for epitaxial Fe_3O_4 growth. Fig. 5.1 (b) showed the XRD scans of Si//Cu 40 nm/ZnCoO 40 nm. Much stronger intensity of (0002) ZnCoO peak was observed, compared to the films grown on SiO_2. To investigate the in-plane orientations, X-ray φ-scans were performed and shown in the inset of Fig. 5.1 (b). Four {111} peaks of the Cu underlayer confirmed that the Cu layer was a (001) epitaxial film. The twelve {10$\bar{1}$1} peaks of the ZnCoO film indicated epitaxial growth with an unusual in-plane 12-fold symmetry.

To further investigate the microstructure of epitaxial ZnCoO films,

we performed the TEM analyses. The direction of the electron beam was tilted along the Cu [110] direction. The dark-field TEM images taken from (1100) and (1100) diffraction patterns, as shown in Fig. 5.2 (a) and (b), respectively, were nearly complementary, which indicated the bi-crystalline nature of epitaxial ZnCoO films. The selected area diffraction (SAD) patterns of ZnCoO, taken on these two different regions by using nano-beam, were shown in Fig. 5.2 (c) (zone axis [1120]) and (d) (zone axis [1100]), respectively. The relationship of crystalline orientations between the Cu and ZnCoO layers was schematically shown in Fig. 5.2 (e). Because the [1120] and [1100] zone axes of ZnCoO wurtzite structure were orthogonal to each other, two kinds of the (0002) epitaxial grains existed (marked as “A” grain and “B” grain in Fig. 5.2 (e), which rotated by 90 degrees with respect to each other along [0001] direction. Therefore, the epitaxial bi-crystalline ZnCoO films showed a 12-fold symmetry in X-ray φ scans.

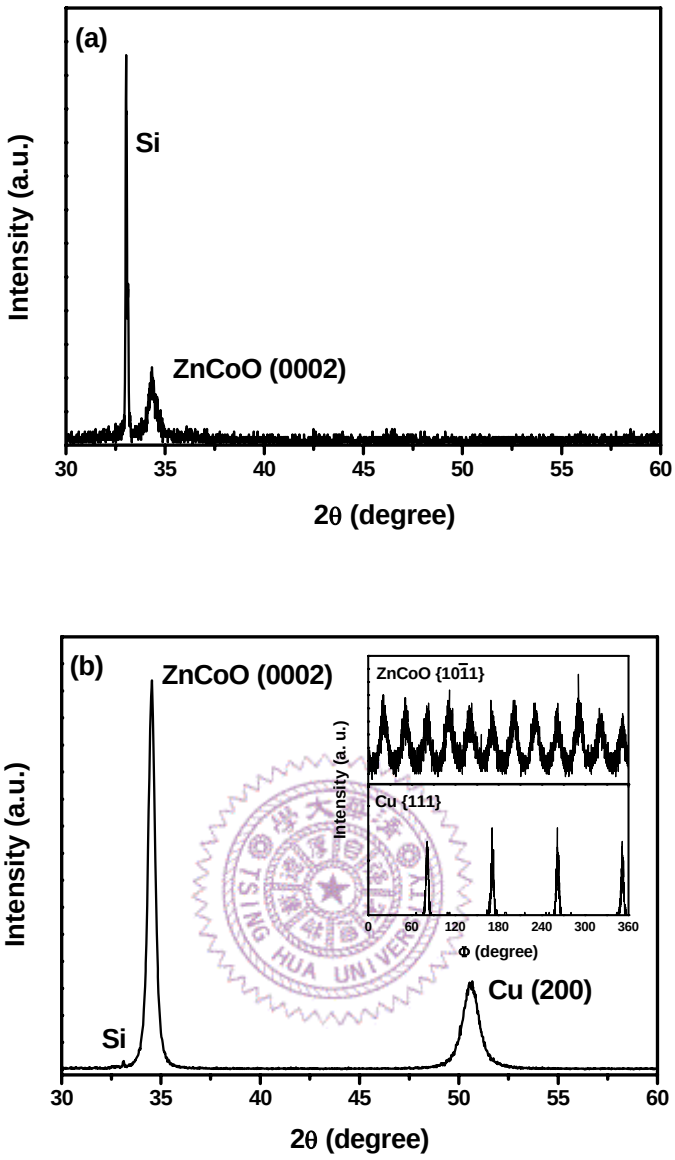

Fig. 5.1. XRD θ-2θ patterns of (a) Si//SiO_2/$ZnCo_{0.07}O$ 40 nm and (b) Si//Cu 40 nm/$ZnCo_{0.07}O$ 40 nm. The inset of Fig. 1 (b) showed the X-ray in-plane φ-scans.

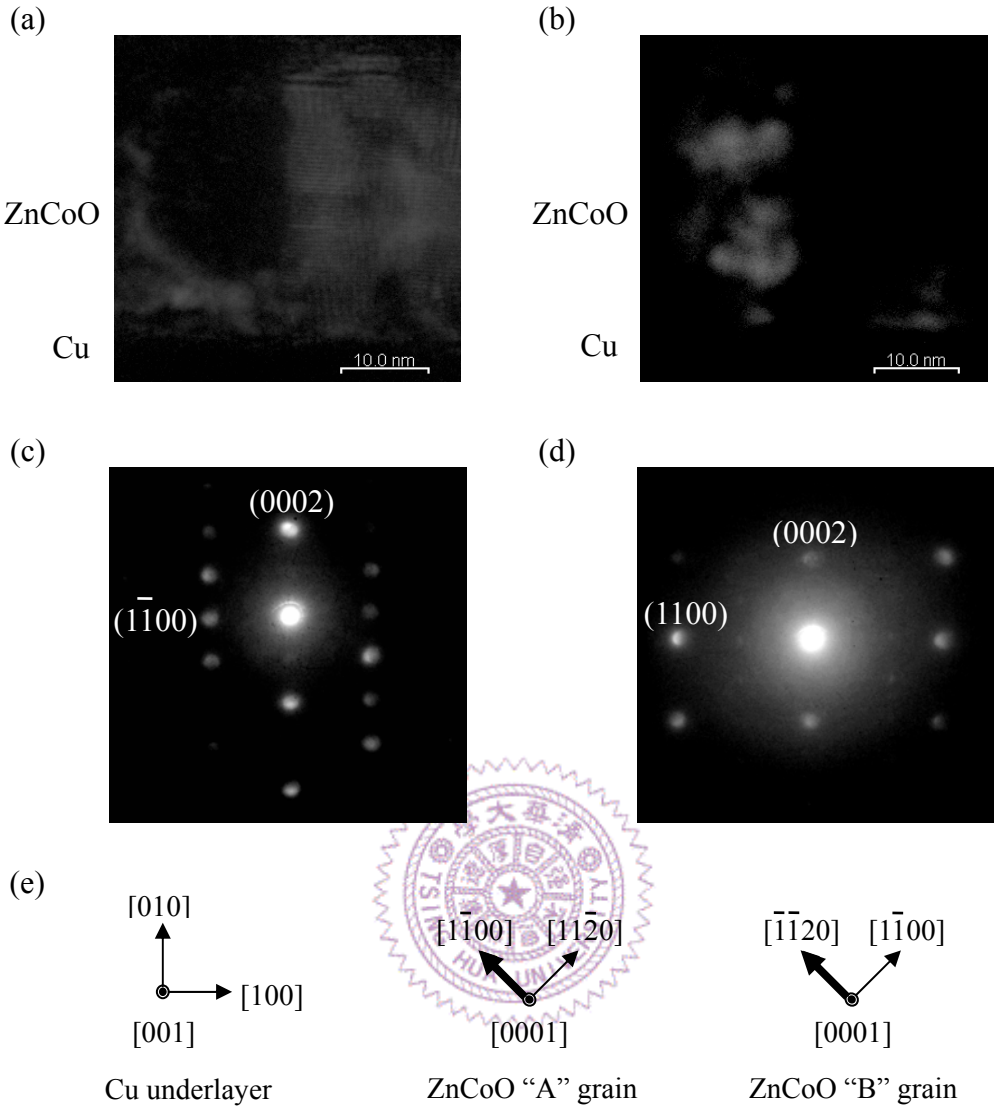

Fig. 5.2. Dark-field TEM images of epitaxial $ZnCo_{0.07}O$ taken from (a) (1100) and (b) (1100) diffraction patterns. SAD patterns taken from (c) A grain (zone axis [1120]) and (d) B grain (zone axis [1100]). The direction of electron beam is along Cu [110]. (e) The schematic diagram of crystalline orientations.

Although the structure of ZnCoO was well characterized, it was quite challenging to only use XRD patterns to conclusively exclude the existence of metallic Co in the film. To rule out the existence of Co clusters, the valence state of Co in $ZnCo_{0.07}O$ was identified by using

XPS with a synchrotron radiation beam. Sample surface was cleaned by cycles of Ar^+ ion sputtering at 1 kV. Cleanliness of the sample surface was confirmed by the absence of a C 1s contamination. The Co core-level 2*p* XPS spectrum of $ZnCo_{0.07}O$ was shown in Fig. 5.3. The spectrum of $ZnCo_{0.07}O$ reveals only $2p^{3/2}$ peak of the Co^{2+} state locating at 781 eV and no metallic Co peak at 778 eV. In addition, no metallic Co clusters can be observed in TEM images. If the room temperature magnetization is contributed from the presence of the metallic Co clusters, the minima cluster size should be larger than 10 nm [15], and it should be visible in TEM images. Only a single phase without clusters was observed in TEM images, which may excluded the possibility that ferromagnetism originated from magnetic clusters. Room-temperature hysteresis loops showed coercivity of 70 Oe. Based on XPS, TEM and SQUID results, we could conclude that room-temperature DMS ZnCoO was obtained by IBD deposited at room temperature.

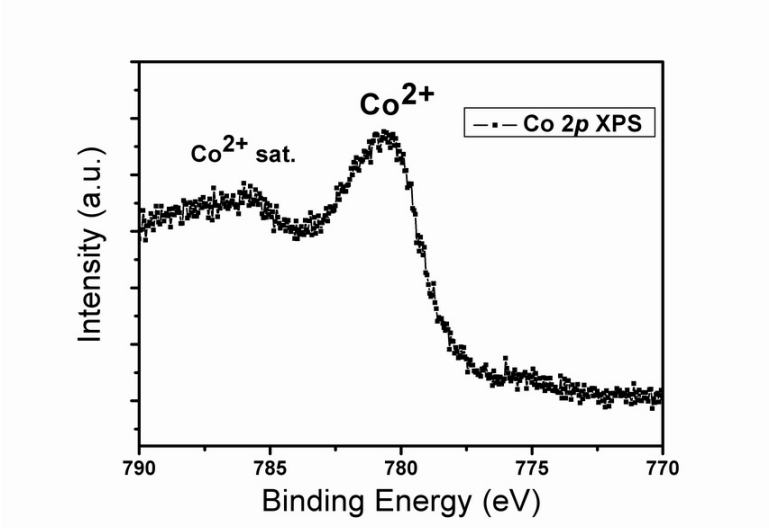

Fig. 5.3. XPS spectrum of the $ZnCo_{0.07}O$.

Hall measurements for samples grown on SiO_2 revealed that ZnCoO films were n-type semiconductors. The carrier concentrations for ZnCoO films deposited at oxygen flow rate of 2 sccm and 3.2 sccm were $6.85\times10^{19}/cm^3$ and $2.31\times10^{19}/cm^3$, respectively. It was reported that Co in ZnO makes deep impurity levels, which trap the electrons emitted by oxygen vacancies, therefore, the carrier concentration was reduced [16]. The lower oxygen flow rate was during ZnCoO deposition, the higher carrier concentration can be obtained, which was ascribed to higher oxygen vacancies

The hysteresis loops measured at 5 K for samples with oxygen flow rate of 2 sccm and 3.2 sccm grown on SiO_2, respectively, are shown in Fig. 5.4. A higher saturation magnetization was obtained for the samples deposited at oxygen flow rate of 2 sccm, which implied that the possible origin of ferromagnetism for our ZnCoO films might be the carrier-mediated mechanism. To further verify the effects of carrier concentration on the ferromagnetism, the samples deposited at oxygen flow rate of 2 sccm was annealed in air at 250 $^{\circ}$C for 1 hr. Both of the carrier concentration and saturation were significantly reduced due to the elimination of oxygen vacancies, which was consistent with the carrier-mediated mechanism. The magneto-resistance (MR) curves, defined as $MR = [R(H) - R(0)]/R(0)$, was measured at 5 K with a magnetic field parallel to the film plane, are shown in Fig. 5.5. A large MR ($>30\%$) of ZnCoO films was observed at 5 K. The positive MR in DMSs was ascribed to the results of giant spin splitting of band states caused by *s-d* exchange interaction [17]. The larger positive MR of

ZnCoO films deposited at lower oxygen flow rate might also result from higher carrier concentration.

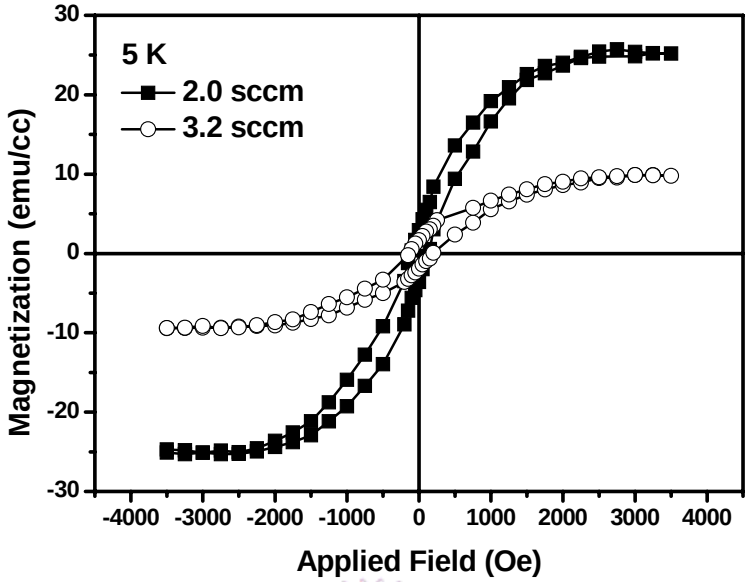

Fig. 5.4. Hysteresis loops, measured at 5 K, of (0002) textured $ZnCo_{0.07}O$ films deposited at different oxygen flow rate.

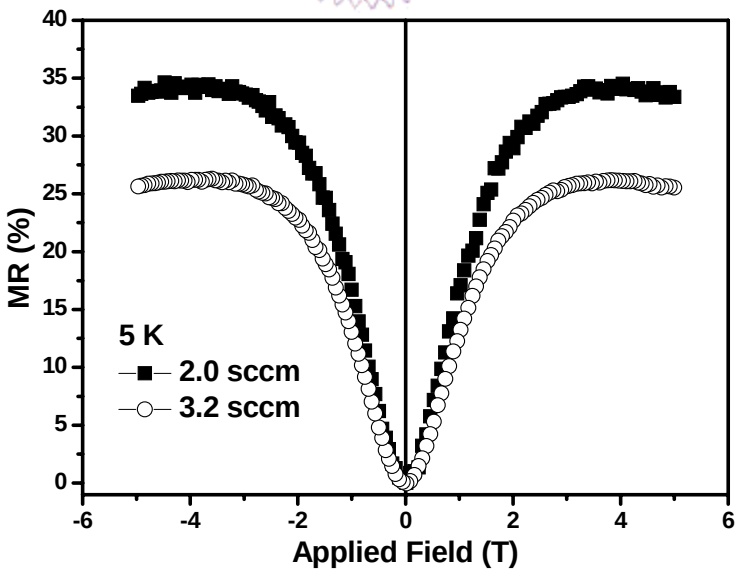

Fig. 5.5. Magneto-resistance of (0002) textured $ZnCo_{0.07}O$ films, measured at 5 K, deposited at different oxygen flow rate.

Since epitaxial films were grown on Cu underlayers, the carrier concentration can not be deduced from our Hall measurement due to current shunting in the Cu layer. Nevertheless, because we used the same recipes as textured films to grow epitaxial ZnCoO films, the carrier concentration should be on the same order of magnitude (~10^{19}/cm^3). The room-temperature hysteresis loop, shown in Fig. 5.6, clearly demonstrated the ferromagnetic characteristic of epitaxial ZnCoO films. Combining the advantages of room-temperature ferromagnetism, high carrier concentrations, and room-temperature growth on Si wafers, epitaxial ZnCoO films fabricated by using IBD can be potentially applied for spintronic devices.

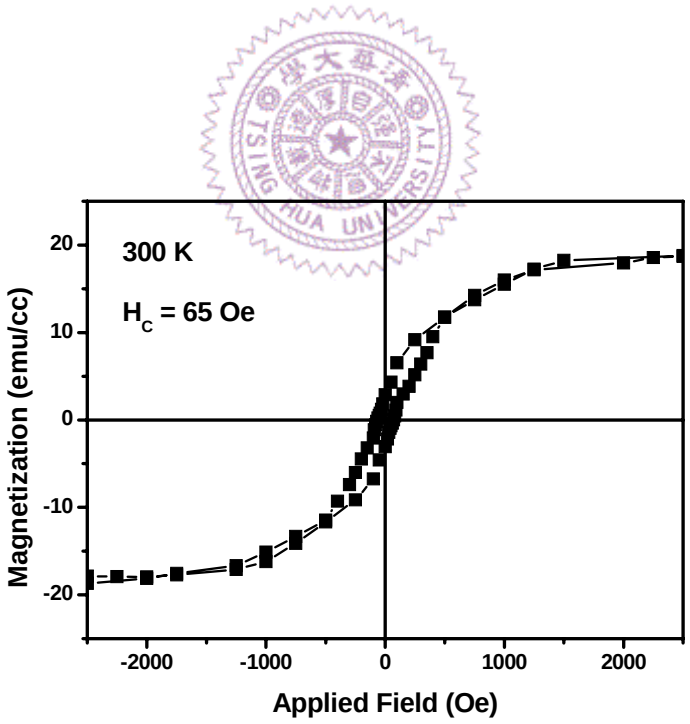

Fig. 5.6. Hysteresis loop of epitaxial (0002) $ZnCo_{0.07}O$ films measured at 300 K.

5.3.b Co-existence of Exchange-bias Fields and Vertical Magnetization Shifts in ZnCoO/NiO System

In the second section, to study exchange bias, samples of Cu 40 nm/ZnCoO 40 nm/ NiO 50 nm were fabricated at room temperature. The XRD patterns, as shown in Fig. 5.7, indicated a good out-of-plane (0002) texture of ZnCoO films and (111) texture of NiO films on (002) Cu underlayers. No second phases were observed in XRD pattern. As mentioned in the pervious section, four {111} peaks of the Cu underlayer, as shown in the inset of Fig. 5.7, confirmed that the Cu layer was a (001) epitaxial film. A 12-fold in-plane symmetry of NiO was also observed, indicating a good epitaxial relationship between ZnCoO and NiO. Since this quasi-epitaxial full-oxide exchange-bias system (ZnCoO/NiO) is prepared at room temperature, we can substantially prevent the problems of interfacial reactions between the DMS and AFM layers.

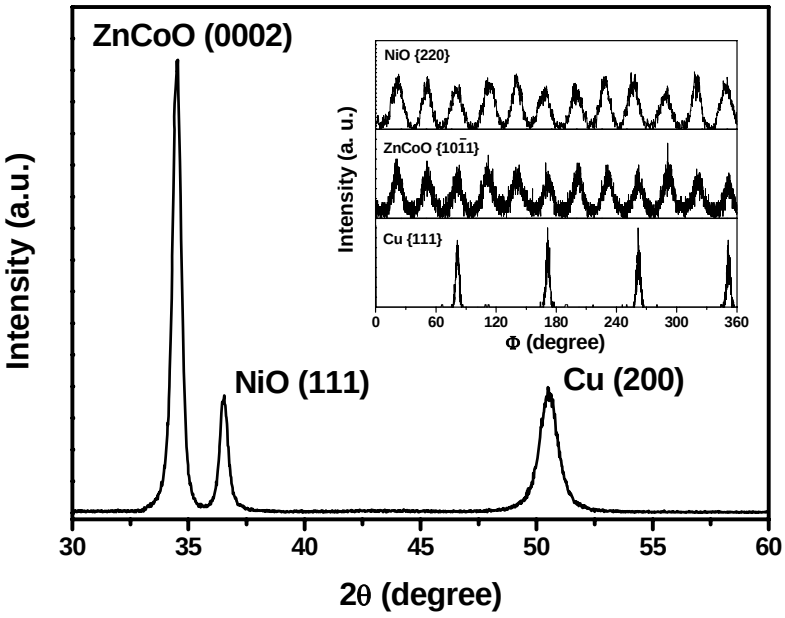

Fig. 5.7. XRD pattern of the Si/Cu/ZnCoO 40nm/ NiO 50nm film. The inset shows the ϕ scans of Cu (200), ZnCoO (10$\bar{1}$1) and NiO (220).

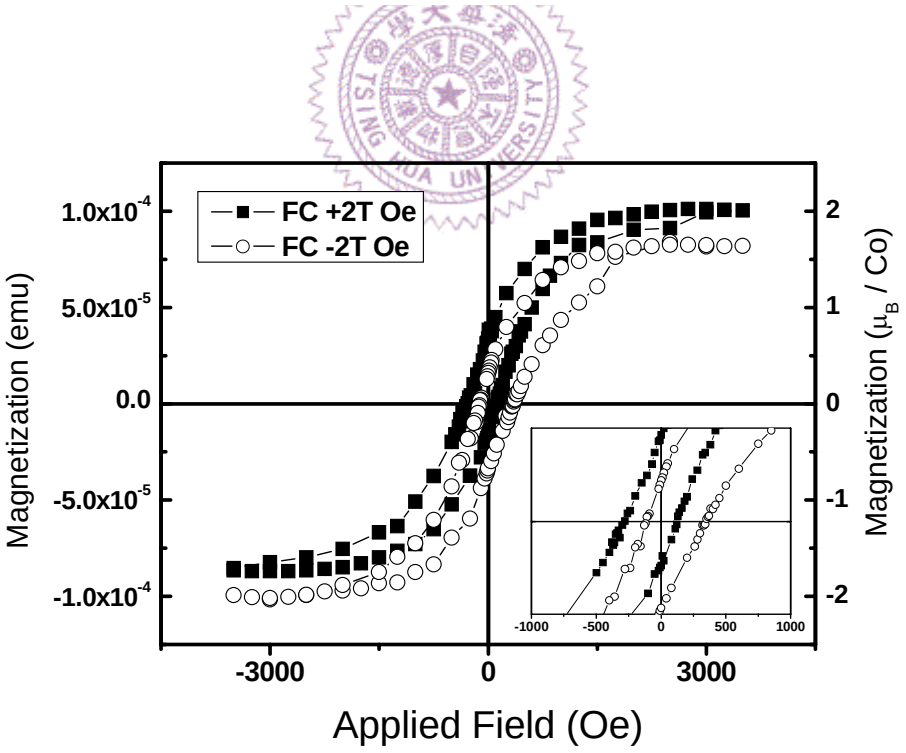

Fig. 5.8. Hysteresis loops measured at 5 K of FC samples of Si/Cu/ZnCoO/NiO with cooling fields of +20000 and -20000 Oe. Inset shows the magnified loops to demonstrate the direction of loop-shifts.

The hysteresis loops of ZnCoO/NiO samples, measured at 5 K through a ZFC process, showed no field or magnetization shifts. The coercivity was 173 Oe, larger than that of ZnCoO films without the NiO layers (115 Oe), measured at 5 K. The enhanced coercivity of ZnCoO/NiO samples indicated the existence of exchange coupling between NiO and ZnCoO. Samples cooled down to 5K in a field of 20000 Oe (FC) showed an exchange field of 120 Oe and a clear vertical magnetization shift, shown in Fig. 5.8. Fig. 5.8 also shows that the direction of the horizontal loop-shift is opposite to the cooling-field direction. Furthermore, the hysteresis loops revealed higher saturation magnetization in the positive-field side when the sample was cooled in a positive field and vice versa for the samples cooled in a negative field. These results implied that both directions of the field-shift and magnetization-shift were determined by the cooling-field direction. Since we would like to prevent the interfacial reactions between NiO and ZnCoO, samples were field-cooled from room temperature instead of from temperatures above the Néel temperature of NiO (T_N = 523 K). In fact, in a previous study of $Ni_{0.52}Co_{0.48}O$/Co system [18], exchange bias could still be established through a field-cooling process with the FC temperature below the Néel temperature of AFM layers; however, the exchange field may be reduced.

In conventional FM/AFM thin-film exchange systems, it is quite unusual to simultaneously observe both field and magnetization shifts. To further investigate the origins, we studied the effects of the cooling field strength on the vertical magnetization shifts and the exchange fields. As shown in Fig. 5.9 (a), both the vertical magnetization shift ΔM (the difference between positive and negative saturation magnetization) and

the exchange field increased with increasing the cooling field. It is worth mentioning that the samples of ZnCoO without NiO layers did not show any magnetization- or field-shifts under the same field-cooling conditions. When the FC field is larger than 500 Oe, a linear dependence of the exchange field on the vertical magnetization shift was observed, shown in Fig. 5.9 (b). In addition to the effects of cooling fields, we also investigated the temperature dependence of the exchange bias field and vertical magnetization shift for the sample field-cooled in 20000 Oe. Exchange-bias fields abruptly dropped as the temperature was increased up to 50K, beyond which the fields decreased slowly, with increasing temperature, shown in Fig. 5.10(a). The magnetization shift shows very similar trend to the exchange field and when the temperature was higher than 50K, the vertical magnetization shift decreased to almost zero. Moreover, exchange bias fields show a linear dependence on vertical magnetization shifts in the low temperature region ($T \leqq 50K$), as shown in Fig 5.10(b). Transitions of the exchange field and ΔM around 50 K may suggest that various mechanisms of the exchange bias exist at different temperature ranges.

To understand this transition, we performed a two-step field-cooling experiment. We first cooled the sample in a field of 20000 Oe from 300K to 50K and then cooled the sample in a zero field from 50K to 5K. Compared to the one-step FC sample from 300K to 5K (H_{ex}=120 Oe), we observed a substantially reduced exchange field of 45 Oe, and no vertical magnetization shift in those two-step FC samples at 5K. The elimination of magnetization shift indicated that the pinned magnetization was mainly

established under 50K with a FC process. This result strongly suggested that the existence of pinned magnetization, which appeared as the magnetization shift, indeed contributed to the exchange fields. How does the pinned magnetization arise? Can it originate from the uncompensated pinned spins of NiO as reported in NiFe/CoO [11] and Co/NiO bilayers [12]? According to Ref. 12, only a small portion (~several percent) of AFM monolayer spins were pinned. If the vertical magnetization shifts mainly resulted from the pinned NiO in our system, the observed magnetization shifts should be orders of magnitude smaller, which may suggest that additional pinned magnetization is needed to explain observed ΔM. Another possible mechanism is the existence of the spin-glass-like (SGL) phase in ZnCoO, of which spins might be "frozen" and aligned in the field cooling direction during a FC process. The complex spin ground state of DMS was reported [19], which may result in the formation of SGL phases. Co-existence of ferromagnetic and spin-glass phases may originate from the local distribution of oxygen vacancies and Co concentration in ZnCoO films [20]. The spins of the SGL phase in ZnCoO were likely "frozen" at the temperatures below 50 K. When the ZnCoO samples without NiO layers were field cooled, although the frozen spins might be aligned by the cooling field, the anisotropy of those regions was too small to keep spins frozen during the reversal of measuring fields; therefore, we did not observe magnetization shifts nor exchange fields. On the other hand, those "frozen" spins might strongly couple to NiO spins, resulting in substantially enhanced anisotropy. Consequently, the magnetization of the SGL phase may not be reversed by the relatively small measuring fields, leading to the

observed co-existence of the magnetization shifts and exchange fields.

A strong dependence of the exchange-coupling strength on the maximum applied field was reported in NiO/Co bilayer systems [21]. Linear dependences of coercivity and uncompensated pinned Ni signal from XMCD on the maximum applied field were observed. The dependences were explained by the existence of SGL phase in the NiO grain boundaries, which can respond to the external fields. As we discussed earlier, the large magnetization shifts in our system excluded the possibility that the major contribution of the vertical shift originated from the NiO layer, but the existence of SGL phase in ZnCoO layers can explain our results: the exchange field and magnetization shift increased with the cooling-field strength, as shown in Fig. 5.9 (a). According to the experiment results, the varied maximum measuring-field, ranging from 3500 to 20000 Oe, did not affect the observed exchange field or ΔM in our system. Instead, the strength of the cooling field played an essential role here. This may suggest that the SGL phase in ZnCoO coupled to NiO possesses high anisotropy at 5K, which is established during the FC process and depends on the cooling-field strength. Furthermore, since the magnetization direction of those "frozen" spins remained unchanged during the magnetization reversal of the rest of ferromagnetic regions of ZnCoO, those spins provided extra pinning sites, in addition to the uncompensated pinned spins in NiO, to maintain the magnetization of ZnCoO in the field-cooling direction. Therefore, when a large cooling-field (>500 Oe) was applied, these frozen spins became the majority of pinning sites. The observed linear dependence of the exchange field on the magnetization shifts, shown in Fig. 5.9 (b), may

strongly indicate that the exchange field is proportional to the number of uncompensated pinned spins.

In addition to the applied field during a FC process, the amount of "frozen" spins can also be a strong function of temperature. Based on two-step-cooling experiments, we knew that the "frozen" spins became a dominated pinning mechanism at temperatures below 50K; therefore, a linear relationship between exchange fields and uncompensated pinned (frozen) magnetization was observed in that temperature range, shown in Fig. 5.10 (b).

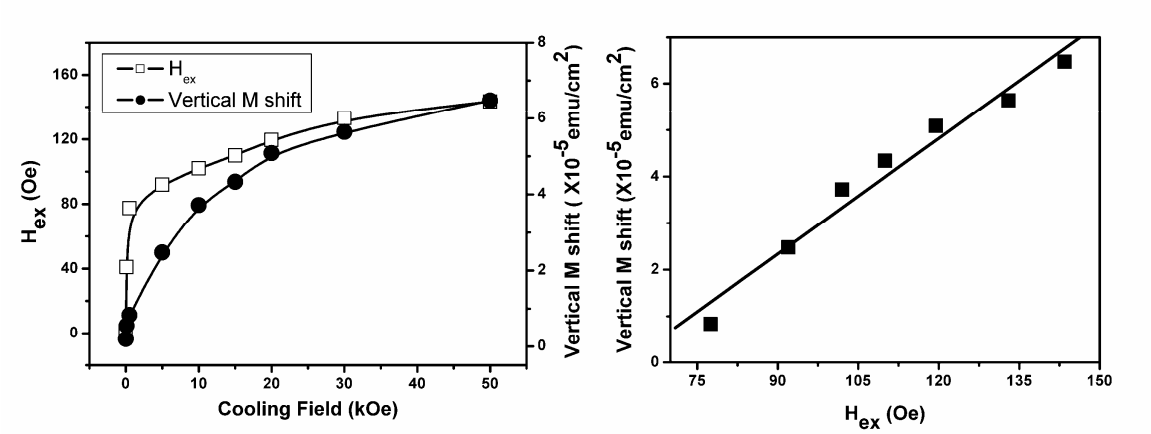

Fig. 5.9. (a) Dependence of exchange bias fields H_{ex} and vertical magnetization shifts on cooling fields. (b) Variation of the exchange bias fields with vertical magnetization shifts for the cooling fields larger than 500 Oe.

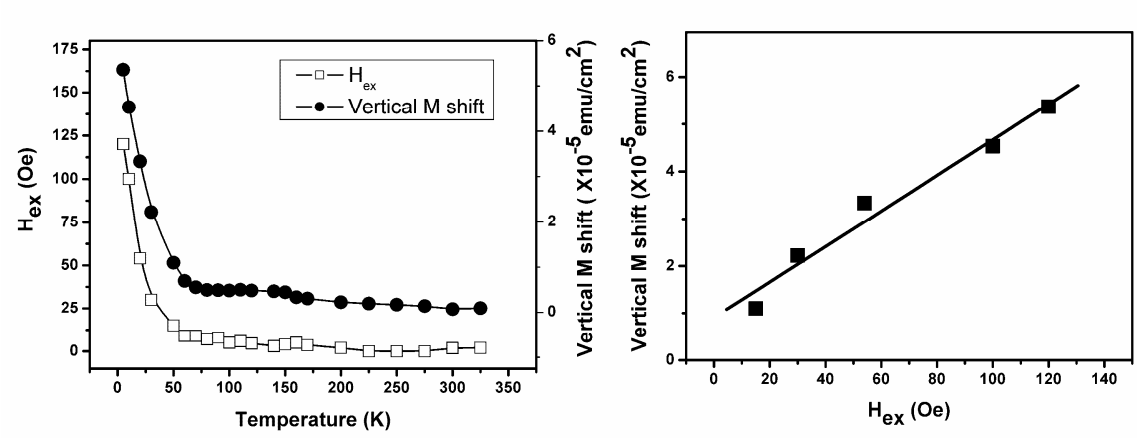

Fig. 5.10. (a) Temperature dependence of exchange bias fields H_{ex} and vertical magnetization shifts. (b) Variation of the exchange bias fields with vertical magnetization shifts for temperatures below 50 K.

5.4 Summary

In the first section of this chapter, we used an IBD system to grow textured and epitaxial $ZnCo_{0.07}O$ films at room temperature on Si wafers. ZnCoO films were n-type semiconductors with high carrier concentrations ($>10^{19}/cm^3$). Higher saturation magnetization and larger positive MR ratio (>30 %) were observed in the ZnCoO films deposited at lower oxygen flow rate, which could be attributed to higher carrier concentrations in these films. The epitaxial (0002) bi-crystalline ZnCoO films were obtained by using Cu underlayers on (001) Si wafers and showed room-temperature ferromagnetism. These diluted magnetic semiconducting ZnCoO films fabricated at room temperature on Si wafers can be easily integrated into conventional processes for future spintronic devices.

In the second section, we simultaneously observed magnetization and field shifts in ZnCoO/NiO bilayers with a FC process. The magnetization shift approached zero and temperature dependences of exchange fields showed a transition around 50 K, indicating that parts of ZnCoO magnetization were pinned through the FC process at temperatures below 50 K. In addition to the exchange coupling between NiO and ferromagnetic ZnCoO, the extra pinning mechanism arises at temperatures below 50 K, plausibly originating from the existence of "frozen" SGL phases, in which spins are strongly coupled to NiO. Those aligned "frozen" spins resulted in the observed magnetization shifts and enhanced exchange fields. Furthermore, the linear dependence of the exchange bias field on the vertical magnetization shift demonstrates that the exchange field is strongly related to the number of pinned uncompensated spins.